RSC Advances

PAPER

View Article Online
View Journal | View Issue

Cite this: *RSC Adv.*, 2023, **13**, 14

Exploring fluoride effects in sterically enhanced cobalt ethylene polymerisation catalysts; a combined experimental and DFT study†

Zilong Li, [a] Yanping Ma, *[ab] Tian Liu,[a] Qiuyue Zhang, [a] Gregory A. Solan,*[b] Tongling Liang [a] and Wen-Hua Sun *[ac]

The fluoro-substituted 2,6-bis(arylimino)pyridine dichlorocobalt complexes, [2-{CMeN(2,6-$(Ph_2CH)_2$-3,4-F_2C_6H)}-6-(CMeNAr)C_5H_3N]$CoCl_2$ (Ar = 2,6-$Me_2C_6H_3$ **Co1**, 2,6-$Et_2C_6H_3$ **Co2**, 2,6-$iPr_2C_6H_3$ **Co3**, 2,4,6-$Me_3C_6H_2$ **Co4**, 2,6-Et-4-MeC_6H_2 **Co5**), were synthesized in good yield from the corresponding unsymmetrical *N*,*N*,*N*′-ligands, **L1–L5**. Besides characterization of **Co1–Co5** by FT-IR spectroscopy, ^{19}F NMR spectroscopy and elemental analysis, the molecular structures of **Co2** and **Co5** were also determined highlighting the unsymmetrical nature of the terdentate ligand and the *pseudo*-square pyramidal geometry about the metal center. When either MAO or MMAO were employed as activators, **Co1–Co5** were able to achieve a wide range of catalytic activities for ethylene polymerisation. **Co5**/MAO exhibited the highest activity of the study at 60 °C (7.6×10^6 g PE mol^{-1} (Co) h^{-1}) which decreased to 3.3×10^6 g PE mol^{-1} (Co) h^{-1} at 80 °C. In addition, it was found that the polymerisation activity increased as the steric hindrance imparted by the *ortho* groups was enhanced (for MMAO: **Co3** > **Co5** > **Co2** > **Co1** > **Co4**), a finding that was supported by DFT calculations. Furthermore, it was shown that particularly high molecular weight polyethylene could be generated (up to 483.8 kg mol^{-1}) when using **Co5**/MMAO at 30 °C, while narrow dispersities (M_w/M_n range: 1.8–4.7) and high linearity (T_m > 131.4 °C) were a feature of all polymers produced. By comparison of **Co3** with its non-fluorinated analogue using experimental data and DFT calculations, the substitution of fluorides at the *meta*- and *para*-positions was demonstrated to boost catalytic activity and improve thermal stability.

Received 15th September 2022
Accepted 25th November 2022

DOI: 10.1039/d2ra05806e

rsc.li/rsc-advances

Introduction

Bis(imino)pyridine-cobalt and -iron complexes have been thoroughly investigated since the late 1990s, due in large part to their ability to promote the polymerisation/oligomerisation of ethylene with high efficiency.[1–3] Against this backdrop, a wide variety of structural variations have been developed that can influence the performance of these late transition metal catalysts and the resulting polymer properties.[4–13] With particular regard to the bis(arylimino)pyridine ligand framework, a good proportion of the developments have focused on systematic changes to the *N*-aryl substituents, with the result that a plethora of different substitution patterns for the *N*-aryl groups now exist.[14–17] Elsewhere, key advances have seen the fusion of cycloalkyl groups to the central pyridine unit, variation of groups on the imine-carbon, and the integration of this *N*,*N*,*N*-ligand into a binucleating framework.[18–21]

In terms of the *N*-aryl substitution pattern, the introduction of sterically hindered groups or electron donating/withdrawing groups to the *ortho*-positions of the *N*-aryl group have proved pivotal in controlling catalytic activity, thermal stability and for the polyethylene generated, molecular weight and various microstructural properties. Likewise, the nature of the substituent on the *para*-position can also be influential on the catalyst performance and polymer properties. For example, Wu's group[22] explored the use of bis(arylimino)pyridine-iron catalysts appended with *N*-2-R^1-4-R^2-6-*sec*-phenethylphenyl groups and found that the nature of both the R^1 and R^2 substituents to be critical to the thermostability of the catalyst and the molecular weight of the polymer.

Over the years, our group has synthesized an assortment of bis(imino)pyridine-iron and -cobalt complexes appended with sterically hindered benzhydryl ($CHPh_2$) groups to the *ortho*- and/or *para*-positions of the *N*-aryl groups (*e.g.* **A–G**, Chart

[a]*Key Laboratory of Engineering Plastics and Beijing National Laboratory for Molecular Sciences, Institute of Chemistry, Chinese Academy of Sciences, Beijing 100190, China. E-mail: myanping@iccas.ac.cn; whsun@iccas.ac.cn*

[b]*Department of Chemistry, University of Leicester, University Road, Leicester LE1 7RH, UK. E-mail: gas8@leicester.ac.uk*

[c]*State Key Laboratory for Oxo Synthesis and Selective Oxidation, Lanzhou Institute of Chemical Physics, Chinese Academy of Sciences, Lanzhou 730000, China*

† Electronic supplementary information (ESI) available: Figures and additional characterization data for ligands, complexes, and resultant polymers; coordinates of all optimized structures by DFT calculations. CCDC 2201737 and 2201738. For ESI and crystallographic data in CIF or other electronic format see DOI: https://doi.org/10.1039/d2ra05806e

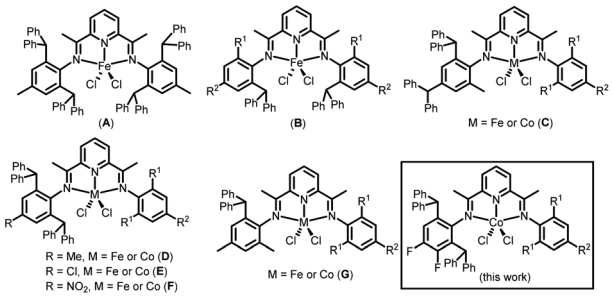

Chart 1 Developments in benzhydryl-containing bis(imino)pyridine-iron and cobalt complexes; R^1 or R^2 = H or alkyl.

1).[5,14,15,23–29] For example, for symmetrical **A**, bearing benzhydryl groups at the 2- and 6-positions, both the iron and cobalt species were inactive for ethylene polymerisation. It was proposed that the huge steric hindrance imparted on both sides of the metal hinders the coordination of ethylene, which makes the polymer chain difficult to propagate. On the other hand, unsymmetrical **C** containing benzhydryl groups at the 2- and 4-positions of just one *N*-aryl group, is highly active but the molecular weight of polyethylene is lowered.[27,28] For its 2,6-substituted comparator **D**, high thermal stability and high ethylene polymerisation activity (22.4×10^6 g PE mol^{-1} (Fe) h^{-1}) are displayed and with the added benefit of no oligomeric fractions.[24] When the *para*-methyl substituent in **D** is substituted with a chloride (**E**), the thermal stability is slightly lower, but the molecular weight of the polyethylene increases.[5]

In this article we set out to develop the 2,6-dibenzhydryl-substituted class of unsymmetrical bis(imino)pyridine-cobalt(II) complex shown for **D–F** (Chart 1). In particular, we were interested in exploring the effect of introducing electron withdrawing fluoride groups at the *para*- and *meta*-positions groups of the $CHPh_2$-substituted *N*-aryl group (Chart 1) on catalyst activity, thermal stability and polymer properties. To allow some fine-tuning, the R^1/R^2 groups on the second *N*-aryl group are systematically varied (*viz.* Me/H, Et/H, i-Pr/H, Me/Me, Et/Me). A comprehensive ethylene polymerisation study is then undertaken that probes the influence of changes in the type/amount of co-catalyst, temperature, pressure and run time. In addition, the synthetic details and characterization data for all ligands and cobalt complexes are disclosed. Finally, DFT calculations are performed to probe the experimental findings and in particular how the introduction of fluoride substituents and sterically hindered *ortho* groups impact on the catalysis.

Results and discussion

Synthesis and characterization of L1–L5 and Co1–Co5

The unsymmetrical bis(imino)pyridines, 2-{CMeN(2,6-$((C_6H_5)_2CH)_2$-3,4-F_2C_6H)}-6-(CMeNAr)C_5H_3N (Ar = 2,6-$Me_2C_6H_3$ **L1**, 2,6-$Et_2C_6H_3$ **L2**, 2,6-i$Pr_2C_6H_3$ **L3**, 2,4,6-$Me_3C_6H_2$ **L4**, 2,6-Et-4-MeC_6H_2 **L5**), were prepared *via* a Schiff base condensation reaction of the corresponding 1-(6(1-(arylimino)ethyl) pyridin-2-yl)ethan-1-one (aryl = 2,6-dimethylphenyl **S1**, 2,6-diethylphenyl **S2**, 2,6-diisopropylphenyl **S3**, 2,4,6-trimethylphenyl **S4**, 2,6-diethyl-4-methylphenyl **S5**) with 2,6-dibenzhydryl-3,4-difluoroaniline in toluene at reflux using *p*-toluenesulfonic acid as the catalyst (Scheme 1).[7,30] All five bis(imino)pyridines have been characterized by IR and multinuclear NMR spectroscopy (^1H, ^{13}C, ^{19}F) and elemental analysis.

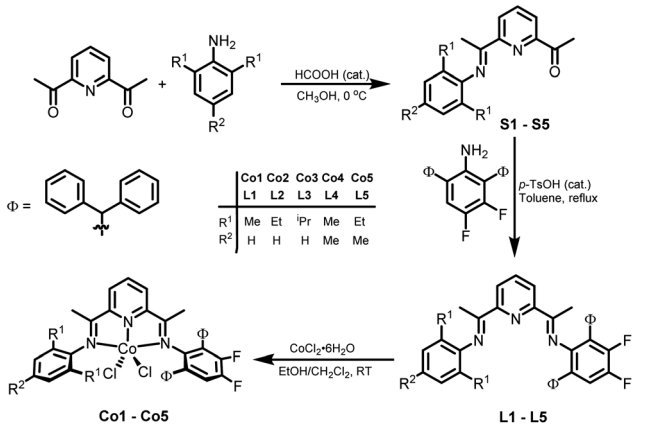

Scheme 1 Preparative routes to **L1–L5** and their cobalt complexes **Co1–Co5**.

Subsequently, the 1 : 1 reaction of cobalt(II) chloride hexahydrate with **L1–L5** in a mixture of solvents composed of dichloromethane and ethanol at room temperature gave on work-up, [2-{CMeN(2,6-$(Ph_2CH)_2$-3,4-F_2C_6H)}-6-(CMeNAr)C_5H_3N]$CoCl_2$ (Ar = 2,6-$Me_2C_6H_3$ **Co1**, 2,6-$Et_2C_6H_3$ **Co2**, 2,6-i$Pr_2C_6H_3$ **Co3**, 2,4,6-$Me_3C_6H_2$ **Co4**, 2,6-Et-4-MeC_6H_2 **Co5**), as green powders in good yields (Scheme 1). All cobalt complexes were characterized by elemental analysis, ^{19}F NMR and FT-IR spectroscopy, while **Co2** and **Co5** were additionally the subject of single crystal X-ray diffraction studies.

In the FT-IR spectra of **L1–L5**, the $\nu_{C=N}$ stretching vibrations appeared in the range 1630–1638 cm^{-1}, while in **Co1–Co5** these bands were shifted to lower wavenumber/intensity (1584–1587 cm^{-1}) as is characteristic of metal coordination.[26,31] Both ligands and complexes gave distinct signals for the *para*- and *meta*-fluoride substituents in their ^{19}F NMR spectra that

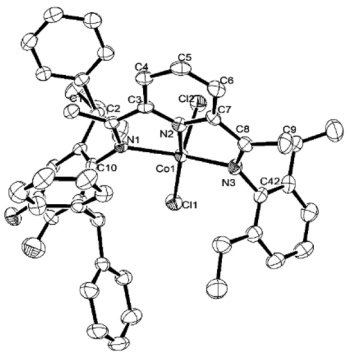

Fig. 1 ORTEP representation of **Co2**. The thermal ellipsoids were set at the 30% probability level, while the hydrogen atoms have been removed for clarity.

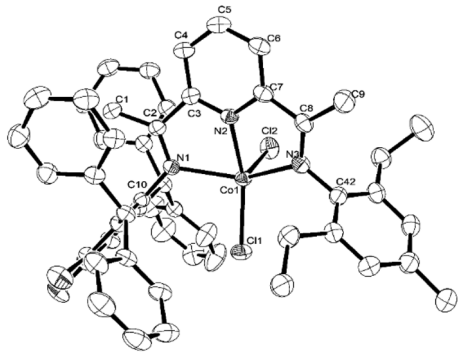

Fig. 2 ORTEP representation of **Co5**. The thermal ellipsoids were set at the 30% probability level, while the hydrogen atoms have been omitted for clarity.

increased in separation on coordination (*e.g.* for **L1** δ −135.2 and −144.3 ppm *vs.* δ −94.5 and −158.3 ppm for **Co1**).

Single crystals of **Co2** and **Co5** were grown as described in the Experimental Section. Perspective views of **Co2** and **Co5** are depicted in Fig. 1 and 2; selected bond lengths and angles are listed in Table 1. The structures of **Co2** and **Co5** are similar differing only in the substitution pattern of one of the *N*-aryl groups (*viz.* 2,6-diethylphenyl **Co2**, 2,6-diethyl-4-methylphenyl **Co5**) and will be described together. Each structure contains a cobalt center coordinated by two chloride ligands and three nitrogen donors from the chelating *N*,*N*,*N*′-ligand to form a distorted square pyramidal geometry. The square base of the pyramid is filled by N1, N2, N3, and Cl1 with Cl2 occupying the apical position. Above the basal plane sits the cobalt atom at a distance of 0.611 Å in **Co2** and 0.556 Å for **Co5**, which is similar to that seen in a number of structurally related analogs.[25,26] Of the three cobalt–nitrogen distances, the central Co–$N_{pyridine}$ bond length [2.077(4) Å for **Co2** and 2.072(3) Å for **Co5**] is the shortest, reflecting the constrictions of the *N*,*N*,*N*′-pincer ligand and the stronger donor properties of the central pyridine unit. The Co–N_{imine} distances although similar in length show some modest variation with Co1–N1 marginally longer than Co1–N4 [2.183(4) *vs.* 2.158(4) Å (**Co2**); 2.220(3) *vs.* 2.180(3) Å (**Co5**)]. These differences are in line with the increased steric attributes of the *N*-2,6-bis(diphenylmethyl)-3,4-difluorophenyl group, while the poorer donor properties of this imine nitrogen due to the electron withdrawing fluoride substituents may also play a contributing factor. As in common for this class of complex, the planes of the *N*-aryl groups are inclined towards perpendicular with respect to the adjacent pyridine unit, as shown by the dihedral angles (75.3°, 88.1°, **Co2**; 74.1°, 88.1°, **Co5**).[25,26] There are no noteworthy intermolecular contacts.

Table 1 Selected bond lengths and angles for **Co2** and **Co5**

	Co2	**Co5**
	Bond length (Å)	
Co1–Cl1	2.2554(14)	2.2565(10)
Co1–Cl2	2.3017(14)	2.3014(10)
Co1–N1	2.183(4)	2.220(3)
Co1–N2	2.077(4)	2.072(3)
Co1–N3	2.158(4)	2.180(3)
	Bond angles (deg)	
N2–Co1–N1	73.21(15)	72.58(11)
N2–Co1–N3	73.72(16)	74.38(11)
N3–Co1–N1	139.31(16)	140.88(11)
N1–Co1–Cl1	97.72(11)	97.08(8)
N1–Co1–Cl2	105.10(11)	102.94(7)
N2–Co1–Cl1	159.25(12)	155.86(8)
N2–Co1–Cl2	91.96(12)	92.48(8)
N3–Co1–Cl1	105.05(13)	104.77(9)
N3–Co1–Cl2	99.04(12)	98.82(8)
Cl1–Co1–Cl2	108.57(6)	111.30(4)

Ethylene polymerisation studies

After a perusal of the literature, it was apparent that nearly all bis(imino)pyridine-cobalt complexes reach optimal catalytic performance for ethylene polymerisation when activated with either modified methylaluminoxane (MMAO) or methylaluminoxane (MAO). Hence, both of these aluminium co-catalysts were used in this work, while **Co5** was chosen as the test precatalyst to permit an optimization of the reaction parameters. Systematic changes in the reaction temperature, Al : Co molar ratio, run time, and ethylene pressure are independently undertaken for both **Co5**/MMAO and **Co5**/MAO systems before extending the corresponding set of optimized conditions to the remaining precatalysts, **Co1–Co4**. Typically, the polymerisation runs were performed in toluene at 10 atm ethylene pressure over 30 min run time; the full set of data are collected in Tables 2 and 3. In all cases, differential scanning calorimetry (DSC) and gel permeation chromatography (GPC)

Table 2 Catalytic evaluation of **Co1–Co5** using MMAO as co-catalyst[a]

Entry	Precat.	Al : Co	*T* (°C)	*t* (min)	Activity[b]	T_m[c] (°C)	M_w[d]	M_w/M_n[d]
1	**Co5**	2000	20	30	2.8	135.6	355.7	2.3
2	**Co5**	2000	30	30	4.2	135.3	483.8	1.8
3	**Co5**	2000	40	30	2.9	135.6	271.2	2.1
4	**Co5**	2000	50	30	1.6	130.3	182.6	2.3
5	**Co5**	2000	60	30	0.5	134.0	145.0	1.9
6	**Co5**	1500	30	30	3.9	135.9	288.2	2.1
7	**Co5**	1750	30	30	4.1	135.3	481.5	1.8
8	**Co5**	2250	30	30	4.4	135.4	412.2	1.8
9	**Co5**	2500	30	30	4.0	135.5	383.3	2.3
10	**Co5**	2750	30	30	3.2	135.3	271.4	1.9
11	**Co5**	2250	30	5	15	136.5	422.6	1.9
12	**Co5**	2250	30	15	6.1	135.2	480.5	1.8
13	**Co5**	2250	30	45	3.0	134.7	511.9	2.2
14	**Co5**	2250	30	60	2.4	135.4	573.2	2.4
15[e]	**Co5**	2250	30	30	2.7	136.2	327.5	3.1
16	**Co1**	2250	30	30	3.3	135.7	274.8	2.1
17	**Co2**	2250	30	30	3.7	135.2	418.3	2.3
18	**Co3**	2250	30	30	4.6	135.1	332.2	2.3
19	**Co4**	2250	30	30	3.0	135.9	253.4	2.8

[a] Conditions: cobalt precatalyst (2.0 μmol), toluene (100 mL), 10 atm ethylene. [b] Activity: 10^6 g PE per mol Co per h. [c] Measured using differential scanning calorimeter (DSC). [d] M_w in kg per mol. M_w and M_w/M_n measured by gel permeation chromatography (GPC). [e] 5 atm.

Table 3 Catalytic evaluation of **Co1–Co5** using MAO as co-catalyst[a]

Entry	Precat.	Al : Co	T (°C)	t (min)	Activity[b]	T_m[c] (°C)	M_w[d]	M_w/M_n[d]
1	**Co5**	1750	40	30	3.3	134.8	132.6	2.5
2	**Co5**	1750	50	30	2.2	132.4	41.2	4.7
3	**Co5**	1750	60	30	7.6	132.2	45.8	3.9
4	**Co5**	1750	70	30	5.6	133.3	48.2	2.8
5	**Co5**	1750	80	30	3.3	133.1	41.5	1.8
6	**Co5**	1250	60	30	3.5	131.4	23.2	3.3
7	**Co5**	1500	60	30	5.4	133.2	33.1	2.2
8	**Co5**	2000	60	30	2.3	132.8	48.3	3.5
9	**Co5**	2250	60	30	2.3	131.9	39.9	3.5
10	**Co5**	1750	60	5	10.8	135.0	38.9	1.9
11	**Co5**	1750	60	15	13.2	135.7	42.3	2.1
12	**Co5**	1750	60	45	6.3	134.6	50.3	2.1
13	**Co5**	1750	60	60	5.3	133.3	62.2	2.3
14[e]	**Co5**	1750	60	30	2.7	132.0	29.4	2.0
15	**Co1**	1750	60	30	1.8	133.3	51.5	3.8
16	**Co2**	1750	60	30	1.9	132.0	30.5	2.2
17	**Co3**	1750	60	30	6.0	135.5	112.5	2.1
18	**Co4**	1750	60	30	2.3	131.4	45.5	3.8

[a] Conditions: cobalt precatalyst (2.0 μmol), toluene (100 mL), 10 atm ethylene. [b] Activity: 10^6 g PE per mol Co per h. [c] Measured using differential scanning calorimeter (DSC). [d] M_w in kg per mol. M_w and M_w/M_n measured by gel permeation chromatography (GPC). [e] 5 atm.

are used to measure various polymer properties (*e.g.* M_w, M_w/M_n and T_m), while high-temperature $^1H/^{13}C$ NMR spectroscopy is employed to explore the microstructural properties of selected polymeric samples.

Catalytic evaluation of Co1–Co5 using MMAO. In order to determine the optimal run temperature, **Co5**/MMAO was initially screened at temperatures between 20 °C and 60 °C with the Al : Co molar ratio fixed at 2000 : 1 (entries 1–5, Table 2). The highest activity of 4.2×10^6 g PE mol^{-1} (Co) h^{-1} was observed at 30 °C which then declined as the temperature was further increased reaching a minimum of 0.5×10^6 g PE mol^{-1} (Co) h^{-1} at 60 °C. It would appear that catalyst deactivation accounts for the loss of activity at higher operating temperatures. The highest molecular weight polyethylene (M_w = 483.8 kg mol^{-1}) was obtained at 30 °C and then steadily fell as the temperature was raised reaching 145.0 kg mol^{-1} at 60 °C (Fig. 3). This finding would suggest that chain transfer becomes more important as the temperature is increased.[31–33] In terms of the polymer dispersities obtained across the temperature range, these remained narrow and unimodal in all cases (M_w/M_n range: 1.8–2.3), indicative of single-site active species.

Subsequently, the influence of the Al : Co molar ratio on catalyst performance and polymer properties was investigated using **Co5**/MMAO (entries 2, 6–10, Table 2). On varying the ratio from 1500 : 1 to 2750 : 1, it was found that the peak polymerisation activity (4.4×10^6 g PE mol^{-1} (Co) h^{-1}) was attained using 2250 equivalents of the co-catalyst. Nonetheless, the range in activities (3.9–4.4×10^6 g PE mol^{-1} (Co) h^{-1}) was narrow which would suggest the amount of co-catalyst employed had limited effect on polymerisation activity. On the other hand, the molecular weight of the polyethylene was more influenced by the Al : Co molar ratio. By increasing the ratio from 1500 : 1 to 2000 : 1, the molecular weight increased reaching a maximum value of 483.8 kg mol^{-1}, whereas at ratios in excess of 2000 : 1, it decreased achieving a value of 271.4 kg mol^{-1} at 2750 : 1 (Fig. 4). This latter observation would suggest that chain transfer from the cobalt catalyst to the alkyl aluminium species starts to become operational with larger amounts of co-catalyst.[17,34,35]

Next, we examined the activity/time profile of **Co5**/MMAO, by performing the polymerisation runs over pre-determined times of 5, 15, 30, 45, and 60 min (entries 8 and 11–14, Table 2); the run temperature and the molar ratio of Al : Co were kept at 30 °C and 2250 : 1, respectively. After 5 min (entry 11, Table 2), the highest activity of 15×10^6 g PE mol^{-1} (Co) h^{-1} was reached, which then subsided reaching a value of 2.4×10^6 g PE mol^{-1} (Co) h^{-1} after 60 min. Indeed, such high activity early in the polymerisation is commonplace in cobalt ethylene polymerisation catalysis with gradual catalyst deactivation considered to occur over longer run times.[7,36]

When the ethylene pressure was reduced from 10 atm to 5 atm (entries 8 and 15 in Table 2), the catalytic activity declined significantly, while the polymer dispersities broadened. Nevertheless, the polyethylene exhibited similar molecular weights over the two different pressures.

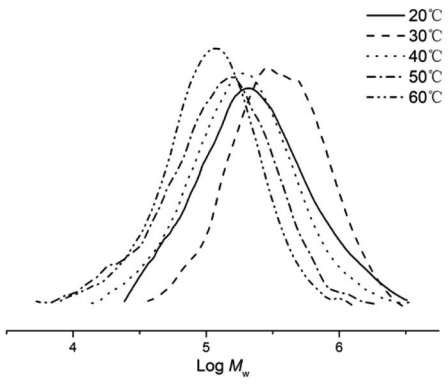

Fig. 3 GPC traces of the polyethylene obtained using **Co5**/MMAO at different temperatures (entries 1–5, Table 2).

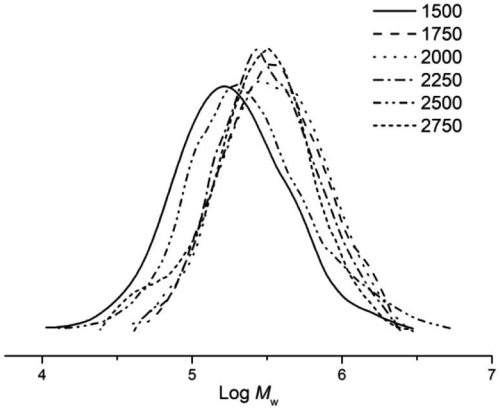

Fig. 4 GPC traces of the polyethylene obtained using **Co5**/MMAO at different Al : Co molar ratios (entries 2, 7–11, Table 2).

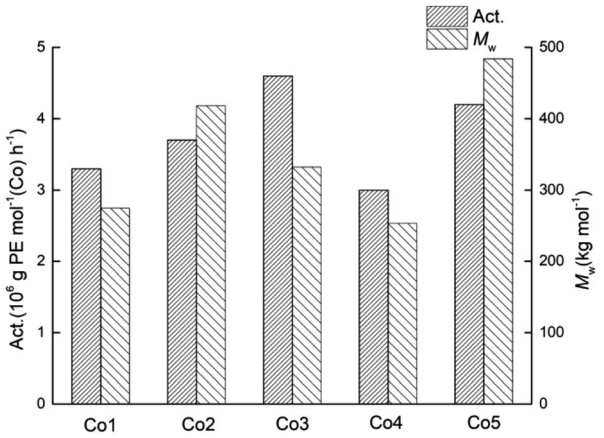

Fig. 5 Variations in catalytic activity and molecular weight of the polyethylene obtained using **Co1–Co5** (entries 8, 16–19, Table 2); MMAO used as the co-catalyst in each case.

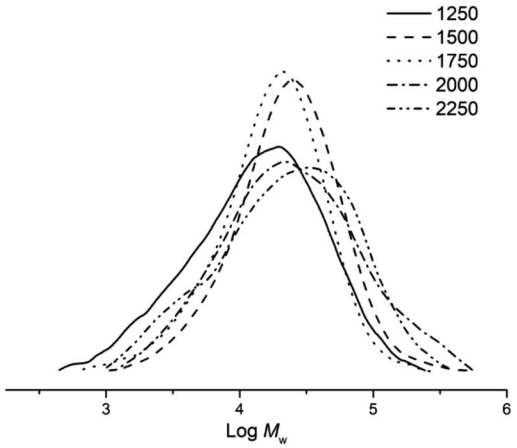

Fig. 6 GPC traces of the polyethylene obtained using **Co5**/MAO at different Al : Co molar ratios (entries 3 and 6–9, Table 3).

On the basis of the most effective set of polymerisation conditions established for **Co5**/MMAO, the performance of the remaining catalysts **Co1–Co4** was then studied (entries 8, 16–19, Table 2). Overall, the catalytic activities for all five complexes fell between 3.0×10^6 g PE mol^{-1} (Co) h^{-1} and 4.6×10^6 g PE mol^{-1} (Co) h^{-1}, with their relative levels decreasing in the order: **Co3** > **Co5** > **Co2** > **Co1** > **Co4** (Fig. 5). Conversely, the impact of the *para*-R^2 group (R^2 = H: **Co1–Co3** *vs.* R^2 = Me: **Co4**, **Co5**) is less obvious. In addition, all catalysts produced high molecular weight polyethylene (253.4–418.3 kg mol^{-1}) with narrow dispersities (M_w/M_n range: 1.8–2.8).

Catalytic evaluation of Co1–Co5 using MAO. To allow a comparison with the MMAO investigation, we also explored using MAO as an activator for all five cobalt precatalysts. Complex **Co5** was again employed as the test catalyst to optimize the conditions; the results of the evaluation are listed in Table 3.

Initially we looked at the effect of the run temperature on the performance of **Co5**/MAO. With the Al : Co molar ratio set at 1750 : 1, the highest activity of 7.6×10^6 g PE mol^{-1} (Co) h^{-1} was reached at 60 °C (entry 3, Table 3). Notably, this catalytic activity far exceeds the maximum level seen for **Co5**/MMAO (4.2×10^6 g PE mol^{-1} (Co) h^{-1}) at 30 °C. Clearly, **Co5**/MAO displays better thermal stability which would point towards the beneficial effects of MAO as a co-catalyst and its impact on the active species. On the other hand, the molecular weight of the polyethylene dropped to 45.8 kg mol^{-1}, which was almost one-tenth of that seen with MMAO. The reason behind this decrease in M_w most likely stems from temperature induced chain transfer.[37] However, when the operating temperature was increased to 80 °C, the activity decreased by more than a half, while the molecular weight of the polymer also decreased (entry 5, Table 3).

With the reaction temperature retained at 60 °C, the Al : Co molar ratio of **Co5**/MAO was incrementally adjusted between 1250 : 1 and 2250 : 1 (entries 3 and 6–9, Table 3). Examination of the data revealed the optimal activity was established with the ratio at 1750 : 1 which coincides with the value selected during the temperature screening step. When the molar ratio was increased above 1750 : 1, the catalytic activity converged to only 30% of the optimal activity (entries 8, 9, Table 3). As for the molecular weight of the polymers, these reached a peak of 48.3 kg mol^{-1} at a ratio of 2000 : 1 and then decreased at higher ratios (Fig. 6), a finding that can be attributed to termination pathway involving chain transfer of the polymer to the co-catalyst.[38,39]

Next the effect of run time on the activity of **Co5**/MAO was investigated with the temperature kept at 60 °C and the molar ratio at 1750 : 1. Dissimilar to the **Co5**/MMAO study, the activity reached a peak after 15 min (13.2×10^6 g of PE mol^{-1} (Co) h^{-1}) and then slowly declined attaining a value of 5.3×10^6 g of PE mol^{-1} (Co) h^{-1} after 1 h (entries 3, 10–13, Table 3). It is evident that **Co5**/MAO displays not only higher activity than **Co5**/MMAO, but also maintains a more uniform activity/time profile and requires a longer induction period to achieve optimal performance.

With the most effective set of conditions identified for **Co5**/MAO (*viz.* Al : Co molar ratio of 1750 : 1, run temperature of 60 °

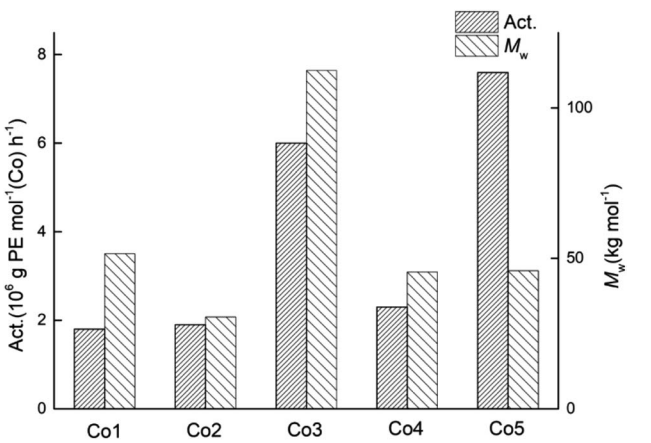

Fig. 7 Variations in catalytic activity and molecular weight of the polyethylene displayed using **Co1–Co5** (entries 3, 15–18, Table 3); MAO used as the co-catalyst in each case.

C, run time of 30 min), the four other cobalt catalysts, **Co1–Co4**, were similarly evaluated; the results are displayed alongside **Co5** in Table 3 (entries 3, 15–18). Inspection of the data revealed that these cobalt catalysts exhibited a wider range in activities spanning from 1.8 to 7.6 $\times$ 10^6 g of PE mol^{-1} (Co) h^{-1} when compared to that found with MMAO (3.0 to 4.6 $\times$ 10^6 g PE mol^{-1} (Co) h^{-1}). In terms of their relative performance, their catalytic activities decreased in the order: **Co5** > **Co3** > **Co4** > **Co2** ~ **Co1** (Fig. 7). This order differs to some degree from that found with MMAO, which plausibly reflects the stability of the active species formed using MMAO over MAO under the higher temperature conditions. Nevertheless, the correlation between steric hindrance and activity remains largely the same with bulkier *ortho*-substituents leading to higher activity. Furthermore, the dispersities of the polymers remained narrow for all five catalysts (M_w/M_n range: 2.1–3.9), highlighting the well-controlled nature of these polymerisations.

Influence of the *para*- and *meta*-fluorides

To appreciate the influence posed by the introduction of fluorides to the *para*- and *meta*-positions of the *N*-aryl group in this work, the activity and molecular weight of **Co3** were compared with those of structurally related cobalt-containing precatalysts **D**,[23] **E**[24] and **F**[25] (Fig. 8); MAO was employed as co-catalyst in each case. At first glance, it is clear that the catalytic systems bearing electron withdrawing *para*-groups (Cl (**E**), NO_2 (**F**) and F (**Co3**)) displayed higher polymerisation activity than with *para*-methyl **D**. With particular regard to **Co3**, this proved the second most productive system (6.0 $\times$ 10^6 g of PE mol^{-1} (Co) h^{-1}) behind Cl-containing **E**, highlighting how variations in electronegativity of the halide can impact on the overall effectiveness of the catalyst. On the other hand, **Co3** produced polyethylene with the lowest molecular weight of this series which relates the relative ease of chain termination.

Microstructural properties of the polyethylene

As given in Tables 2 and 3, the melting points displayed by the polyethylenes fell between 130.3 °C and 136.5 °C, which is characteristic of highly linear polyethylene.[16,17,30] In order to confirm this and obtain more information about their microstructural properties (*e.g.* polymer end groups and branching), representative samples obtained using **Co5**/MAO and **Co5**/MMAO have been analyzed by ^{1}H and ^{13}C NMR spectroscopy (recorded in tetrachloroethane-d_2 at 100 °C).

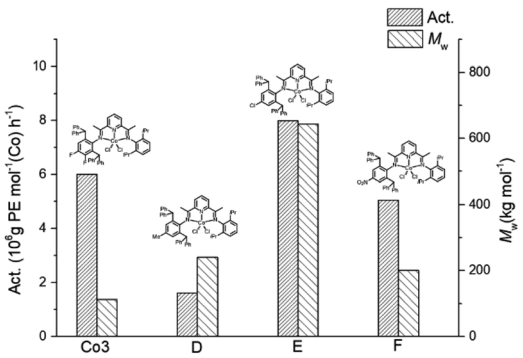

Fig. 8 Comparison of catalytic activity and polymer molecular weight obtained using Co3 and that for cobalt-containing D, E, F; MAO used as a co-catalysts in each case under comparable polymerisation conditions.

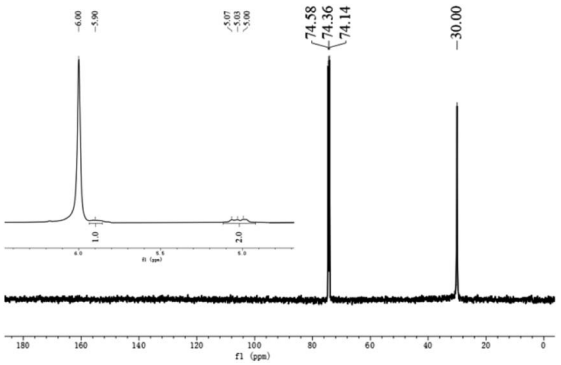

Fig. 9 ^{13}C NMR spectrum of the polyethylene obtained using **Co5**/MAO along with an inset showing the vinylic region of its ^{1}H NMR spectrum (entry 3, Table 3); both spectra were recorded in tetrachloroethane-d_2 at 100 °C.

For the polymer sample produced using **Co5**/MAO (M_w = 45.8 kg mol^{-1}; entry 3, Table 3), the ^{13}C NMR spectrum revealed as the only visible resonance for the polymer, a high-intensity singlet at δ 30.00 ppm assignable to the –$(CH_2)_n$– repeat unit in line with the high linearity of the material (Fig. 9). By contrast, the ^{1}H NMR spectrum gave information on end group composition with downfield resonances typical of an alkenyl chain group end (RCH = CH_2). This observation indicates that β-H elimination or β-H transfer provides a key chain termination pathway.[37] It is uncertain why the ^{13}C NMR spectrum did not reveal vinylic carbons but may relate to the strength of the sample and solubility.

Additionally, the polymer sample with higher molecular weight prepared using **Co5**/MMAO (M_w = 412.2 kg mol^{-1}; entry 8, Table 2) was characterized by ^{13}C NMR spectroscopy (Fig. S22†). Once again the only detectable signal was for the –$(CH_2)_n$– repeat unit at δ 29.60 ppm. However, in this case the ^{1}H NMR spectrum showed no evidence for vinylic protons which is likely due to the higher molecular weight of this sample.

DFT calculations

To study the influence of the *para*- and *meta*-fluoride substituents in **Co3** along with the steric hindrance exerted by the *ortho* groups on the catalytic activity, the ethylene insertion pathway was computed by DFT calculations using the M06/6-31G** method. In previous works, active catalysts can be generated by treating Co(I) and Co(II) species with strong Lewis acid activators like MAO, but the oxidation state of the active species is still unclear.[40–42] In this study we are concerned with making a comparison of the transition state that contain a coordinated ethylene and alkyl group.

As a cationic cobalt-alkyl species can display higher catalytic activity than its neutral counterpart,[43] we selected cationic

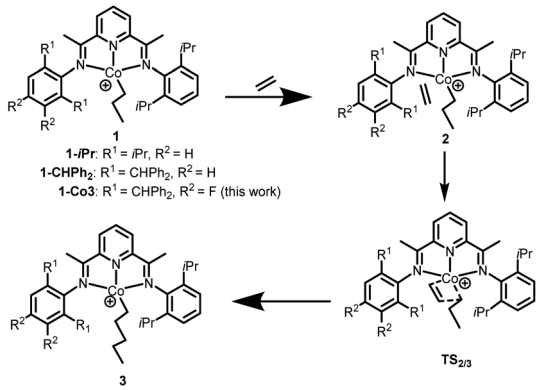

Scheme 2 Intermediates and transition states involved in the proposed reaction pathway: 1 + C_2H_4 → 2 → $TS_{2/3}$ → 3.

cobalt-alkyl species **1** in Scheme 2 (*viz.* **1-iPr**, **1-CHPh$_2$** and **1-Co3**) as the starting structure to react with the ethylene. The chain propagated structure **3** was produced *via* coordinated intermediate **2** and transition state **TS$_{2/3}$**. The Gibbs energy profiles of the reaction pathways (Scheme 2) for the three cobalt species are displayed in Fig. 10 (left, middle and right); both the doublet and quartet states were calculated. On inspection of the figure, is apparent that the doublet state possesses a lower energy than the quartet state in most cases. Exceptionally, the chain propagated intermediate **3-iPr** is particularly stable in its quartet state (ΔG −43.44 kcal mol^{-1}), as has been found in our previous calculations.[43] On the other hand, a similar finding is not observed where the system contains the more sterically demanding $CHPh_2$ groups in the *ortho* positions. It would seem plausible that the catalysts incorporating $CHPh_2$ groups (**1-CHPh$_2$** and **1-Co3**) induce a less stable intermediate that reacts further to generate polymers with higher molecular weight.

In terms of the energy barriers for the ethylene insertion step (*i.e. via* **TS$_{2/3}$**), these were found to decrease in the order: **iPr** (7.72 kcal mol^{-1}) > **CHPh$_2$** (6.69 kcal mol^{-1}) > **Co3** (5.56 kcal mol^{-1}). This would suggest that the increase in the steric hindrance at the *ortho*-positions makes the barrier to ethylene insertion more facile, leading to higher polymerisation activity. Furthermore, the relatively lower barrier in **Co3** over **CHPh$_2$** would suggest the electron withdrawing fluorides in the *meta* and *para* positions are contributing cooperatively with the bulky $CHPh_2$ groups. Moreover, these computational results support the experimental observations, where the catalytic activities for these three systems follow the order: **Co3** (6.0 × 10^6 g of PE mol^{-1} (Co) h^{-1}) > **CHPh$_2$** (1.8 × 10^6 g of PE mol^{-1} (Co) h^{-1}) > **iPr** (4.6 × 10^5 g of PE mol^{-1} (Co) h^{-1}).[1]

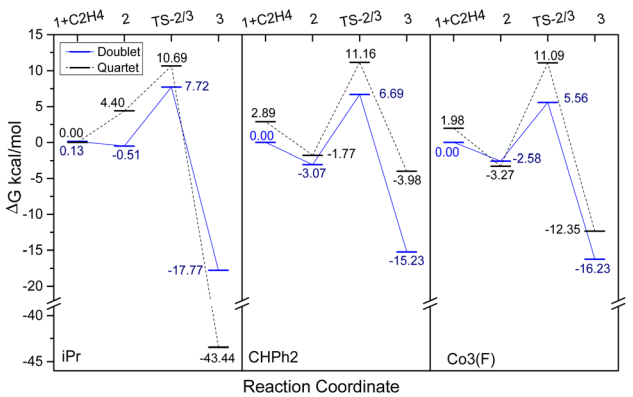

Fig. 10 The Gibbs energy profiles for the ethylene insertion pathway 1 + C_2H_4 → 2 → $TS_{2/3}$ → 3, using **1-iPr** (left) **1-CHPh$_2$** (middle) and **1-Co3** (right) as shown Scheme 2. Units in kcal mol^{-1}.

Conclusions

In summary, the bis(arylimino)pyridine dichlorocobalt complexes, **Co1–Co5**, comprising one *N*-2,6-bis(diphenylmethyl)-3,4-difluorophenyl group and one sterically variable *N*-aryl group have been successfully synthesized. In addition, all five complexes and their ligand precursors have been fully characterized including in the cases of **Co2** and **Co5** by single crystal X-ray diffraction. On activation with either MAO or MMAO, all complexes showed good catalytic activity for ethylene polymerisation forming highly linear polyethylenes with narrow dispersities (M_w/M_n range: 1.8–4.7); vinyl-end groups were identified for lower molecular weight samples. Notably, it was found that the polymerisation activity was enhanced with an increase of the steric hindrance at the *ortho* positions which was further supported by DFT calculations. Moreover, the highest activity (7.6 × 10^6 g PE mol^{-1} (Co) h^{-1}) was achieved at 60 °C for **Co5**/MAO, highlighting the appreciable thermal stability of this catalyst. On the other hand, the highest molecular weight polymer (483.8 kg mol^{-1}) was achieved using **Co5**/MMAO at 30 °C. On the basis of experimental data and DFT calculations for **Co3** and its non-fluorinated analogue, the substitution of fluorides at the *meta*- and *para*-positions was shown to enhance catalytic activity and raise thermal stability.

Experimental

General considerations

All experimental operations that make use of compounds which are sensitive to air and/or moisture were performed under a nitrogen atmosphere using standard Schlenk techniques. The toluene used for the ethylene polymerisation evaluation was heated to reflux over sodium for at least 10 h before distillation was undertaken under a nitrogen atmosphere. Methylaluminoxane (MAO, 1.38 M in toluene) and modified methylaluminoxane (MMAO, 1.93 M in heptane) were provided by Albemarle Corp. High purity ethylene was provided by Beijing Yanshan Petrochemical Company and used as received. Other reagents were purchased from Aldrich, Acros or local suppliers. The ^{1}H, ^{13}C NMR and ^{19}F NMR spectroscopic measurements for **L1–L5** as well as the ^{19}F NMR spectra for cobalt complexes **Co1–Co5** were performed on a Bruker DMX 400 and 500 MHz (^{19}F NMR) instrument at room temperature using TMS as an internal standard for ^{1}H/^{13}C NMR and CF_3COOH as an external standard. All chemical shifts and coupling constants are given in ppm and in Hz, respectively. Elemental analyses (C, H and N)

Table 4 Crystallographic data and structure refinement for Co2 and Co5

	Co2	Co5
Crystal colour	Brown	Brown
Empirical formula	$C_{52}H_{47}Cl_4CoF_2N_3$	$C_{53}H_{49}Cl_4CoF_2N_3$
Formula weight	952.65	966.68
Temperature/K	170.00(11)	169.97(11)
Crystal system	Monoclinic	Monoclinic
Space group	*Cc*	*Cc*
a/Å	23.8272(3)	24.2166(3)
b/Å	14.5493(2)	14.6821(2)
c/Å	16.0514(2)	16.4823(2)
α/°	90	90
β/°	125.0950(10)	127.0490(10)
γ/°	90	90
Volume/Å^3	4552.89(11)	4677.22(11)
Z	4	4
ρ_{calc} g cm^{-3}	1.39	1.373
μ/mm^{-1}	5.498	5.36
F(000)	1972	2004
Crystal size/mm^3	0.15 × 0.1 × 0.05	0.15 × 0.12 × 0.08
2Θ range for data collection/°	7.582 to 150.576	7.562 to 150.714
Index ranges	$-29 \le h \le 29$, $-18 \le k \le 14$ $-19 \le l \le 19$	$-30 \le h \le 30$, $-17 \le k \le 18$ $-19 \le l \le 20$
Reflections collected	16 783	16 345
Independent reflections	7537 [$R_{int} = 0.0351$, $R_{sigma} = 0.0390$]	5983 [$R_{int} = 0.0268$, $R_{sigma} = 0.0267$]
Data/restraints/parameters	7537/2/563	5983/2/573
Goodness-of-fit on F^2	1.041	1.027
Final *R* indexes [$I >= 2\sigma(I)$]	$R_1 = 0.0509$, w$R_2 = 0.1403$	$R_1 = 0.0379$, w$R_2 = 0.1039$
Final *R* indexes [all data]	$R_1 = 0.0523$, w$R_2 = 0.1416$	$R_1 = 0.0389$, w$R_2 = 0.1046$
Largest diff. peak/hole/*e* Å^{-3}	2.66/−0.61	1.38/−0.49

were performed on a Flash EA 1112 microanalyzer. FT-IR spectra were recorded using a PerkinElmer System 2000 FT-IR spectrometer. The molecular weights and molecular weight distributions (M_w/M_n) of the polyethylenes were measured using a PL-GPC220 instrument at 160 °C with 1,2,4-trichlorobenzene as the solvent. Data collection and processing were performed using Cirrus GPC Software (Beijing, China) and Multi Detector Software (Beijing, China). The calibrants employed for constructing conventional calibration (Polystyrene Calibration KitS-M-10) were provided by PL Company (Beijing, China). The true average molecular weights of polyethylene were achieved by inputting the Mark-Houwink constants of polyethylene; K (0.727) and α (40.6) were provided by PL Company (Beijing, China). The samples were dissolved at a concentration of 1.0 to 2.5 mg mL^{-1} depending on the molecular weights. The DSC traces and melting points of the polyethylene were obtained from the second scanning run on a PerkinElmer TA-Q2000 DSC analyzer under a nitrogen atmosphere. During the procedure, a sample of about 4.0–6.0 mg was heated to 160 °C at a heating rate of 20 °C min^{-1}, followed by 5 min at 150 °C to remove the thermal history and then cooled at a rate of 20 °C min^{-1} to −20 °C. High temperature ^{1}H and ^{13}C NMR spectra of the polyethylenes were recorded on a Bruker DMX 500 MHz instrument at 100 °C in deuterated 1,1,2,2-tetrachloroethane with TMS as an internal standard. All computational work was carried out by density functional theory (DFT) using the Gaussian 09 software.[44] A hybrid *meta*-GGA level density functional M06 (ref. 45) in conjunction with 6-31G** basis set was adopted for all atoms. Solvent effect was considered for the fully optimized structures by using the integral equation formalism polarizable continuum model (IEFPCM)[46] with the radii and cavity-dispersion-solvent structure terms given in Truhlar and co-workers' SMD solvation model[47] for the solvent effect correction of toluene: $\varepsilon = 2.3741$. An ultrafine integration grid (99 590) was used for numerical integrations. Thermal corrections were calculated within the harmonic potential approximation on optimized structures under $T = 298.15$ K and 1 atm pressure. The keto-imine compounds, 1-(6(1-(arylimino)ethyl) pyridin-2-yl)ethan-1-one (aryl = 2,6-dimethylphenyl **S1**, 2,6-diethylphenyl **S2**, 2,6-diisopropylphenyl **S3**, 2,4,6-trimethylphenyl **S4**, 2,6-diethyl-4-methylphenyl **S5**), were prepared according to literature routes *via* the interaction of 2,6-diacetylpyridine with the corresponding aniline in methanol with formic acid as promoter at 0 °C.[48]

Synthesis of 2-{CMeN(2,6-(Ph$_2$CH)$_2$-3,4-F$_2$C$_6$H)}-6-(CMeNAr)C$_5$H$_3$N. (a) Ar = 2,6-Me$_2$C$_6$H$_3$ **L1**. To a round bottomed flask containing toluene (100 mL) was added a mixture of **S1** (0.54 g, 2.00 mmol), 2,6-dibenzhydryl-3,4-difluoroaniline (1.38 g, 3.00 mmol) and a catalytic amount of *p*-toluenesulfonic acid. The resulting solution was stirred at reflux for 6 h. After cooling to room temperature, the solvent was evaporated under reduced pressure and the residue purified by alumina column chromatography (100/1 petroleum ether/ethyl acetate), affording **L1** as a green powder (0.59 g, 42%). FT-IR (cm^{-1}): 3030(w), 2962(w), 2918(w), 1949(w), 1636(m), 1596(m), 1495(m), 1473(m), 1447(m), 1416(m), 1364(m), 1322(m), 1259(s), 1199(m),

1075(vs), 1014(vs), 931(m), 864(m), 798(vs), 764(vs), 695(vs). ^{1}H NMR (400 MHz, $CDCl_3$, TMS): δ 8.46–8.44 (d, J = 7.2 Hz 1H, Py-H), 8.23–8.21 (d, J = 7.2 Hz, 1H, Py), 7.91–7.87 (t, J = 7.8 Hz, 1H, Py), 7.31–6.74 (m, 24H, Ph), 5.40 (s, 1H, –C*H*Ph_2), 5.31 (s, 1H, –C*H*Ph_2), 2.10 (s, 3H, CH_3), 2.06–2.05 (d, J = 4.0 Hz, 6H, CH_3), 1.10 (s, 3H, CH_3). ^{13}C NMR (100 MHz, $CDCl_3$, TMS): δ 169.95, 165.10, 153.12, 152.48, 146.64, 142.96, 141.02, 140.64, 139.59, 138.35, 134.81, 127.67, 126.50, 126.46, 126.29, 126.00, 125.89, 124.54, 124.48, 124.14, 123.37, 123.33, 121.05, 120.35, 120.20, 49.86, 47.16, 15.93, 15.12, 14.34. ^{19}F NMR (470 MHz, $CDCl_3$): δ −135.6, −144.1. Anal. calcd. for $C_{49}H_{41}F_2N_3$ (709.88): C, 82.91; H, 5.82; N, 5.92. Found: C, 82.86; H, 5.74; N, 5.88%.

(b) Ar = 2,6-$Et_2C_6H_3$ **L2**. Using a similar procedure as described for **L1** but with **S2** as the ketone, **L2** was isolated as a green powder (0.54 g, 37%). FT-IR (cm^{-1}): 3028(w), 2963(m), 2935(w), 2869(w), 1970(w), 1631(m), 1595(m), 1494(m), 1475(m), 1447(m), 1420(m), 1366(m), 1321(w), 1292(m), 1261(s), 1193(m), 1080(s), 1017(s), 925(m), 865(m), 797(vs), 767(s), 743(m), 696(vs). ^{1}H-NMR (400 MHz; $CDCl_3$, TMS): δ 8.44–8.42 (d, J = 7.6 Hz 1H, Py-H), 8.23–8.21 (d, J = 7.6 Hz, 1H, Py), 7.91–7.87 (t, J = 7.8 Hz, 1H, Py), 7.30–6.73 (m, 24H, Ph), 5.40 (s, 1H, –C*H*Ph_2), 5.31 (s, 1H, –C*H*Ph_2), 2.48–2.30 (m, 4H, –*H*$_2$CH$_3$), 2.11 (s, 3H, CH_3), 1.18–1.13 (m, 6H, CH_3), 1.11 (s, 3H, CH_3). ^{13}C NMR (100 MHz; $CDCl_3$; TMS): δ 169.92, 164.80, 153.08, 152.42, 145.63, 140.96, 140.58, 139.54, 138.30, 134.76, 129.07, 129.03, 127.61, 127.21, 126.42, 126.39, 126.22, 125.94, 124.47, 124.41, 124.07, 123.87, 121.28, 120.25, 120.08, 119.96, 119.85, 114.67, 49.79, 47.10, 22.49, 15.07, 14.64, 11.66. ^{19}F NMR (470 MHz, $CDCl_3$): δ −135.6, −144.1. Anal. calcd. for $C_{51}H_{45}F_2N_3$ (737.94): C, 83.01; H, 6.15; N, 5.69. Found: C, 82.92; H, 5.95; N, 5.62%.

(c) Ar = 2,6-i$Pr_2C_6H_3$ **L3**. Using a similar procedure as described for **L1** but with **S3** as the ketone, **L3** was isolated as a green powder (0.84 g, 22%). FT-IR (cm^{-1}): 3060(w), 3027(w), 2960(m), 2923(w), 2866(w), 1947(w), 1637(m), 1605 w), 1575(w), 1494(m), 1473(s), 1449(s), 1420(m), 1365(m), 1324(m), 1244(m), 1194(m), 1104(s), 1078(s), 1003(m), 967(m), 930(m), 907(w), 861(w), 818(m), 792(m), 765(s), 695(vs). ^{1}H NMR (400 MHz; $CDCl_3$, TMS): δ 8.43–8.41 (d, J = 7.6 Hz 1H, Py-H), 8.22–8.20 (d, J = 7.6 Hz, 1H, Py), 7.91–7.87 (t, J = 7.8 Hz, 1H, Py), 7.31–6.76 (m, 24H, Ph), 5.34 (s, 1H, –C*H*Ph_2), 5.31 (s, 1H, –C*H*Ph_2), 2.79–2.12 (m, 2H, –*H*$_2$(CH$_3$)$_2$), 2.12 (s, 3H, CH_3), 1.19–1.16 (m, 12H, CH_3), 1.12 (s, 3H, CH_3). ^{13}C NMR (100 MHz, $CDCl_3$, TMS): δ 169.99, 164.91, 153.12, 152.48, 144.35, 140.99, 140.61, 139.59, 138.34, 134.81, 133.73, 133.69, 127.66, 127.25, 126.46, 126.42, 126.26, 125.98, 124.51, 124.45, 124.12, 121.58, 120.98, 120.33, 120.10, 120.00, 49.79, 49.84, 47.14, 26.26, 21.20, 20.87, 20.85, 15.12, 15.04. ^{19}F NMR (470 MHz, $CDCl_3$): δ −135.6, −144.1. Anal. calcd. for $C_{53}H_{49}F_2N_3$ (765.99): C, 83.11; H, 6.45; N, 5.49. Found: C, 82.94; H, 6.27; N, 5.36%.

(d) Ar = 2,4,6-$Me_3C_6H_2$ **L4**. Using a similar procedure as described for **L1** but with **S4** as the ketone, **L4** was isolated as a green powder (0.26 g, 7%). FT-IR (cm^{-1}): 3030(w), 2959(w), 2913(w), 2880(vw), 2162(w), 1973(w), 1639(s), 1602(m),1 566(m), 1472(s), 1447(m), 1417(m), 1363(m), 1322(m), 1261(m), 1214(m), 1145(m), 1111(s), 1077(s), 1005(s), 931(m), 905(m), 854(m), 817(s), 794(s), 744(m), 696(vs). ^{1}H NMR ($CDCl_3$, TMS): δ 8.44–8.42 (d, J = 7.6 Hz, 1H, Py-H), 8.21–8.19 (d, J = 7.6 Hz, 1H, Py), 7.89–7.85 (t, J = 7.8 Hz, 1H, Py), 7.30–6.73 (m, 23H, Ph), 5.39 (s, 1H, –C*H*Ph_2), 5.30 (s, 1H, –C*H*Ph_2), 2.30 (s, 3H, CH_3), 2.09 (s, 3H, CH_3), 2.02–2.01 (d, J = 4.4 Hz, 6H, CH_3), 1.10 (s, 3H, CH_3). ^{13}C NMR (100 MHz, $CDCl_3$, TMS): δ 169.99, 165.31, 153.28, 152.45, 144.15, 141.05, 140.66, 139.61, 138.37, 134.78, 130.26, 127.68, 127.28, 126.57, 126.51, 126.47, 126.30, 126.01, 124.54, 124.49, 124.15, 123.23, 123.18, 120.35, 120.13, 114.93, 114.75, 49.87, 47.17, 18.72, 15.86, 15.14, 14.30. ^{19}F NMR (470 MHz, $CDCl_3$): δ −135.6, −144.1. Anal. calcd. for $C_{50}H_{43}F_2N_3$ (723.91): C, 82.96; H, 5.99; N, 5.80. Found: C, 82.82; H, 5.87; N, 5.74%.

(e) Ar = 2,6-Et_2-4-MeC_6H_2 **L5**. Using a similar procedure as described for **L1** but with **S5** as the ketone, **L5** was isolated as a green powder (0.45 g, 30%). FT-IR (cm^{-1}): 3029(w), 2963(m), 2932(w), 2870(w), 1953(w), 1638(s), 1602(m), 1566(m), 1494(m), 1475(s), 1450(s), 1420(m), 1363(s), 1322(m), 1296(m), 1260(m), 1243(m), 1221(m), 1296(m), 1260(m), 1243(m), 1221(m), 1208(m), 1146(m), 1118(s), 1076(s), 1007(m), 931(m), 863(m), 802(s), 764(m), 744(m), 697(vs). ^{1}H NMR ($CDCl_3$, TMS): δ 8.43–8.41 (d, J = 7.2 Hz 1H, Py-H), 8.21–8.19 (d, J = 7.6 Hz, 1H, Py), 7.89–7.86 (t, J = 7.8 Hz, 1H, Py), 7.30–6.75 (m, 23H, Ph), 5.39 (s, 1H, –C*H*Ph_2), 5.30 (s, 1H, –C*H*Ph_2), 2.39–2.31 (m, 3H, CH_3), 2.36 (s, 4H, –*H*$_2$CH$_3$), 2.10 (s, 3H, CH_3), 1.25–1.12 (m, 6H, –CH$_2$C*H*$_3$), 1.11 (s, 3H, CH_3). ^{13}C NMR (100 MHz, $CDCl_3$, TMS): δ 165.03, 153.25, 152.41, 141.00, 140.62, 139.58, 138.34, 134.75, 130.44, 128.97, 127.65, 127.24, 126.46, 126.42, 126.25, 125.97, 124.63, 124.45, 124.10, 120.27, 120.04, 49.82, 22.52, 18.95, 15.11, 14.62, 11.80. ^{19}F NMR (470 MHz, $CDCl_3$): δ −135.6, −144.1. Anal. calcd. for $C_{52}H_{47}F_2N_3$ (751.97): C, 83.06; H, 6.30; N, 5.59%. Found: C, 83.14; H, 6.15; N, 5.66%.

Synthesis of [2-{CMeN(2,6-$(Ph_2CH)_2$-3,4-F_2C_6H)}-6-(CMeNAr)C_5H_3N]$CoCl_2$. (a) Ar = 2,6-$Me_2C_6H_3$ **Co1**. Under a nitrogen atmosphere, a mixture of **L1** (0.11 g, 0.15 mmol), $CoCl_2 \cdot 6H_2O$ (0.027 g, 0.12 mmol), dichloromethane (10 mL) and ethanol (5 mL) was stirred at room temperature for 6 h. All volatiles were then removed under reduced pressure to give a concentrated solution. An excess of diethyl ether was added to induce precipitation and the precipitate collected by filtration and washed with diethyl ether (3 × 10 mL) yielding **Co1** as a green powder (0.065 g, 64%). FT-IR (KBr, cm^{-1}): 3064(w), 3027(w), 2958(w), 2918(w), 2860(w), 2158(w), 1971(w), 1622(m), 1585(m), 1494(s), 1474(s), 1427(m), 1372(m), 1325(m), 1261(s), 1217(m), 1085(m), 1008(m), 939(m), 913(w), 860(w), 813(m), 768(s), 704(vs). ^{19}F NMR (470 MHz, $CDCl_3$): δ −94.5, −158.3. Anal. calcd. for $C_{49}H_{41}F_2N_3Cl_2Co$ (839.72): C, 70.09; H, 4.92; N, 5.00. Found: C, 69.88; H, 5.13; N, 4.87%.

(b) Ar = 2,6-$Et_2C_6H_3$ **Co2**. The synthesis of **Co2** was carried out using a procedure and molar ratios similar to that described for **Co1**, but with **L2** used in place of **L1**. Following work-up, **Co2** was isolated as a green powder (0.095 g, 94%). FT-IR (KBr, cm^{-1}): 3063(w), 2972(w), 2937(w), 2878(w), 2161(m), 1974(w), 1617(w), 1587(m), 1496(m), 1476(s), 1449(m), 1424(m), 1365(m), 1324(m), 1266(m), 1207(m), 1078(m), 1007(m), 940(m), 862(m), 812(m), 770(s), 739(m), 703(vs). ^{19}F NMR (470 MHz, $CDCl_3$): δ −93.1, −158.0. Anal. calcd. for $C_{51}H_{45}F_2N_3Cl_2Co$ (867.77): C, 70.59; H, 5.23; N, 4.84. Found: C, C, 70.34; H, 5.45; N, 4.74%.

(c) Ar = 2,6-$iPr_2C_6H_3$ **Co3**. The synthesis of **Co3** was carried out using a procedure and molar ratios similar to that described for **Co1**, but with **L3** used in place of **L1**. Following work-up, **Co3** was isolated as a green powder (0.051 g, 94%). FT-IR (KBr, cm^{-1}): 3057(w), 2961(m), 2920(w), 2866(w), 2161(w), 1971(w), 1584(m), 1495(m), 1473(s), 1450(s), 1371(m), 1323(m), 1269(m), 1208(m), 1103(m), 1078(m), 1028(m), 1003(m), 938(m), 863(w), 806(m), 769(s), 699(vs). ^{19}F NMR (470 MHz, $CDCl_3$): δ −92.5, −157.6. Anal. calcd. for $C_{53}H_{49}F_2N_3Cl_2Co$ (895.83): C, 71.06; H, 5.51; N, 4.69. Found: C, 70.96; H, 5.57; N, 4.64%.

(d) Ar = 2,4,6-$Me_3C_6H_2$ **Co4**. The synthesis of **Co4** was carried out using a procedure and molar ratios similar to that described for **Co1**, but with **L4** used in place of **L1**. Following work-up, **Co4** was isolated as a green powder (0.038 g, 50%). FT-IR (KBr, cm^{-1}): 3061(w), 3034(w), 2951(w), 2923(w), 2916(w), 2840(w), 2160(w), 1974(w), 1617(w), 1588(m), 1496(m), 1477(s), 1449(m), 1425(m), 1365(m), 1325(m), 1265(m), 1221(m), 1196(m), 1079(m), 1009(m), 939(w), 858(m), 816(m), 771(m), 736(m), 703(vs). ^{19}F NMR (470 MHz, $CDCl_3$): δ −94.7, −158.0. Anal. calcd. for $C_{50}H_{43}F_2N_3Cl_2Co$ (853.75): C, 70.34; H, 5.08; N, 4.92. Found: C, 70.12; H, 5.23; N, 4.74%.

(e) Ar = 2,6-Et_2-4-MeC_6H_2 **Co5**. The synthesis of **Co5** was carried out using a procedure and molar ratios similar to that described for **Co1**, but with **L5** used in place of **L1**. Following work-up, **Co5** was isolated as a green powder (0.13 g, 94%). FT-IR (KBr, cm^{-1}): 3032(w), 2972(w), 2925(w), 2878(w), 2162(w), 1974(w), 1619(w), 1586(m), 1496(m), 1477(s), 1449(m), 1423(m), 1363(m), 1325(m), 1263(s), 1219(m), 1078(m), 1031(m), 1010(m), 939(m), 862(m), 814(m), 7701(s), 735 (s), 702(vs). ^{19}F NMR (470 MHz, $CDCl_3$): δ −93.3, −157.9. Anal. calcd. for $C_{52}H_{47}F_2N_3Cl_2Co$ (881.80): C, 70.83; H, 5.37; N, 4.77. Found: C, 70.74; H, 5.59; N, 4.55%.

X-ray crystallographic studies

Single crystals of **Co2** and **Co5** for X-ray diffraction studies were grown by diffusing diethyl ether onto dichloromethane solutions of the corresponding complex at ambient temperature. By employing a XtaLAB Synergy R HyPix diffractometer equipped with graphite monochromated Cu-Kα radiation (λ = 1.54184 Å) at 173(2) K, cell parameters were obtained by global refinement of the positions of all collected reflections. Intensities were corrected for Lorentz and polarization effects and empirical absorption. Structure solution was performed by direct methods and refined by full-matrix least squares on F^2. All non-hydrogen atoms were refined anisotropically and all hydrogen atoms were placed in calculated positions. Using Olex2,[49] the structure was solved by the SHELXT[50] structure solution program employing Intrinsic Phasing by and refined with the SHELXL[51] refinement package using the Least Squares minimization. Details of the X-ray structure determinations and refinements are provided in Table 4.

Conflicts of interest

There are no conflicts to declare.

Acknowledgements

This work was supported by the National Natural Science Foundation of China (No. 21871275). G.A.S. thanks the Chinese Academy of Sciences for a President's International Fellowship for Visiting Scientists. Y. M. thanks the Chinese Academy of Sciences for the support of her visiting scholarship to the UK.

Notes and references

1 G. J. P. Britovsek, V. C. Gibson, B. S. Kimberley, P. J. Maddox, S. J. McTavish, G. A. Solan, A. J. P. White and D. J. Williams, *Chem. Commun.*, 1998, 7, 849.
2 B. L. Small, M. Brookhart and A. M. A. Bennett, *J. Am. Chem. Soc.*, 1998, **120**, 4049.
3 G. J. P. Britovsek, M. Bruce, V. C. Gibson, B. S. Kimberley, P. J. Maddox, S. Mastroianni, S. J. McTavish, C. Redshaw, G. A. Solan, S. Strömberg, A. J. P. White and D. J. Williams, *J. Am. Chem. Soc.*, 1999, **121**, 8728.
4 V. C. Gibson, C. Redshaw and G. A. Solan, *Chem. Rev.*, 2007, **107**, 1745.
5 X. Cao, F. He, W. Zhao, Z. Cai, X. Hao, T. Shiono, C. Redshaw and W.-H. Sun, *Polymer*, 2012, **53**, 1870.
6 M. Han, Q. Zhang, I. I. Oleynik, H. Suo, I. V. Oleynik, G. A. Solan, Y. Ma, T. Liang and W.-H. Sun, *Catalysts*, 2020, **10**, 1002.
7 Q. Zhang, Z. Li, M. Han, J. Xiang, G. A. Solan, Y. Ma, l. tongling and W.-H. Sun, *Catal. Sci. Technol.*, 2020, **11**, 656.
8 F. Huang, Q. Xing, T. Liang, Z. Flisak, B. Ye, X. Hu, W. Yang and W.-H. Sun, *Dalton Trans.*, 2014, **43**, 16818.
9 Z. Wang, R. Zhang, W. Zhang, G. A. Solan, Q. Liu, T. Liang and W.-H. Sun, *Catal. Sci. Technol.*, 2019, **9**, 1933.
10 W. Zhang, S. Wang, S. Du, C.-Y. Guo, X. Hao and W.-H. Sun, *Macromol. Chem. Phys.*, 2014, **215**, 1797.
11 C. Bariashir, Z. Wang, S. Du, G. A. Solan, C. Huang, T. Liang and W.-H. Sun, *J. Polym. Sci., Part A: Polym. Chem.*, 2017, **55**, 3980.
12 S. Ahmed, W. Yang, Z. Ma and W.-H. Sun, *J. Phys. Chem. A*, 2018, **122**, 9637.
13 V. K. Appukuttan, Y. Liu, B. C. Son, C.-S. Ha, H. Suh and I. Kim, *Organometallics*, 2011, **30**, 2285.
14 Q. Mahmood, J. Guo, W. Zhang, Y. Ma, T. Liang and W.-H. Sun, *Organometallics*, 2018, **37**, 957.
15 Q. Mahmood, E. Yue, J. Guo, W. Zhang, Y. Ma, X. Hao and W.-H. Sun, *Polymer*, 2018, **159**, 124.
16 F. Huang, W. Zhang, E. Yue, T. Liang, X. Hu and W.-H. Sun, *Dalton Trans.*, 2016, **45**, 657.
17 H. Suo, I. I. Oleynik, C. Bariashir, I. V. Oleynik, Z. Wang, G. A. Solan, Y. Ma, T. Liang and W.-H. Sun, *Polymer*, 2018, **149**, 45.
18 Y. Huang, R. Zhang, T. Liang, X. Hu, G. A. Solan and W.-H. Sun, *Organometallics*, 2019, **38**, 1143.
19 C. Bariashir, Z. Wang, G. A. Solan, C. Huang, X. Hao and W.-H. Sun, *Polymer*, 2019, **171**, 87.
20 Q. Xing, T. Zhao, Y. Qiao, L. Wang, C. Redshaw and W.-H. Sun, *RSC Adv.*, 2013, **3**, 26184.

21 Q. Chen, W. Zhang, G. A. Solan, R. Zhang, L. Guo, X. Hao and W.-H. Sun, *Organometallics*, 2018, **37**, 4002.
22 L. Guo, H. Gao, L. Zhang, F. Zhu and Q. Wu, *Organometallics*, 2010, **29**, 2118.
23 J. Yu, W. Huang, L. Wang, C. Redshaw and W.-H. Sun, *Dalton Trans.*, 2011, **40**, 10209.
24 J. Yu, H. Liu, W. Zhang, X. Hao and W. H. Sun, *Chem. Commun.*, 2011, **47**, 3257.
25 F. He, W. Zhao, X.-P. Cao, T. Liang, C. Redshaw and W.-H. Sun, *J. Organomet. Chem.*, 2012, **713**, 209.
26 Q. Mahmood, Y. Ma, X. Hao and W.-H. Sun, *Appl. Organomet. Chem.*, 2019, **33**, e4857.
27 W. Zhao, J. Yu, S. Song, W. Yang, H. Liu, X. Hao, C. Redshaw and W.-H. Sun, *Polymer*, 2012, **53**, 130.
28 J. Lai, W. Zhao, W. Yang, C. Redshaw, T. Liang, Y. Liu and W.-H. Sun, *Polym. Chem.*, 2012, **3**, 787.
29 C. Bariashir, R. Zhang, A. Vignesh, Y. Ma, T. Liang and W.-H. Sun, *ACS Omega*, 2021, **6**, 4448.
30 R. Zhang, Y. Ma, M. Han, G. A. Solan, Y. Pi, Y. Sun and W.-H. Sun, *Appl. Organomet. Chem.*, 2019, **33**, e5157.
31 M. Han, Q. Zhang, I. I. Oleinik, H. Suo, G. A. Solan, I. V. Oleinik, Y. Ma, T. Liang and W.-H. Sun, *Dalton Trans.*, 2020, **49**, 4774.
32 M. Han, I. I. Oleynik, Y. Ma, I. V. Oleynik, G. A. Solan, T. Liang and W.-H. Sun, *Appl. Organomet. Chem.*, 2021, **35**, e6429.
33 R. Zhang, Y. Huang, G. A. Solan, W. Zhang, X. Hu, X. Hao and W.-H. Sun, *Dalton Trans.*, 2019, **48**, 8175.
34 J. Guo, W. Zhang, I. I. Oleynik, G. A. Solan, I. V. Oleynik, T. Liang and W.-H. Sun, *Dalton Trans.*, 2020, **49**, 136.
35 Q. Zhang, R. Zhang, M. Han, W. Yang, T. Liang and W.-H. Sun, *Dalton Trans.*, 2020, **49**, 7384.
36 T. Liu, Y. Ma, G. A. Solan, T. Liang and W.-H. Sun, *Appl. Organometal. Chem.*, 2021, **35**, e6259.
37 R. Zhang, Y. Huang, Y. Ma, G. A. Solan, X. Hu, T. Liang and W.-H. Sun, *Polymer*, 2021, **222**, 123684.
38 H. Suo, I. I. Oleynik, C. Bariashir, I. V. Oleynik, Z. Wang, G. A. Solan, Y. Ma, T. Liang and W.-H. Sun, *Polymer*, 2018, **149**, 45.
39 L. Guo, M. Zada, W. Zhang, A. Vignesh, D. Zhu, Y. Ma, T. Liang and W.-H. Sun, *Dalton Trans.*, 2019, **48**, 5604.
40 P. Margl, L. Deng and T. Ziegler, *Organometallics*, 1999, **18**, 5701.
41 K. P. Tellmann, M. J. Humphries, H. S. Rzepa and V. C. Gibson, *Organometallics*, 2004, **23**, 5503.
42 I. E. Soshnikov, N. V. Semikolenova, A. N. Bushmelev, K. P. Bryliakov, O. Y. Lyakin, C. Redshaw, V. A. Zakharov and E. P. Talsi, *Organometallics*, 2009, **28**, 6003.
43 Z. Li, Y. Ma and W.-H. Sun, *Catalysts*, 2020, **10**, 1396.
44 M. J. Frisch, G. W. Trucks, H. B. Schlegel, G. E. Scuseria, M. A. Robb, J. R. Cheeseman, G. Scalmani, V. Barone, B. Mennucci, G. A. Petersson, H. Nakatsuji, M. Caricato, X. Li, H. P. Hratchian, A. F. Izmaylov, J. Bloino, G. Zheng, J. L. Sonnenberg, M. Hada, M. Ehara, K. Toyota, R. Fukuda, J. Hasegawa, M. Ishida, T. Nakajima, Y. Honda, O. Kitao, H. Nakai, T. Vreven, J. A. Montgomery Jr, J. E. Peralta, F. Ogliaro, M. Bearpark, J. J. Heyd, E. Brothers, K. N. Kudin, V. N. Staroverov, T. Keith, R. Kobayashi, J. Normand, K. Raghavachari, A. Rendell, J. C. Burant, S. S. Iyengar, J. Tomasi, M. Cossi, N. Rega, J. M. Millam, M. Klene, J. E. Knox, J. B. Cross, V. Bakken, C. Adamo, J. Jaramillo, R. Gomperts, R. E. Stratmann, O. Yazyev, A. J. Austin, R. Cammi, C. Pomelli, J. W. Ochterski, R. L. Martin, K. Morokuma, V. G. Zakrzewski, G. A. Voth, P. Salvador, J. J. Dannenberg, S. Dapprich, A. D. Daniels, O. Farkas, J. B. Foresman, J. V. Ortiz, J. Cioslowski, and D. J. Fox, *Gaussian 09, Revision E.01*, Gaussian, Inc., Wallingford, CT, 2013.
45 Y. Zhao and D. G. Truhlar, *J. Chem. Phys.*, 2006, **125**, 194101.
46 B. Mennucci, Tomasi and R. Cammi, *Chem. Rev.*, 2005, **105**, 2999.
47 A. V. Marenich, C. J. Cramer and D. G. Truhlar, *J. Phys. Chem. B*, 2009, **113**, 6378.
48 C. Bianchini, G. Mantovani, A. Meli, F. Migliacci, F. Zanobini, F. Laschi and A. Sommazzi, *Eur. J. Inorg. Chem.*, 2003, **8**, 1620.
49 O. V. Dolomanov, L. J. Bourhis, R. J. Gildea, J. A. K. Howard and H. Puschmann, *J. Appl. Crystallogr.*, 2009, **42**, 339.
50 G. M. Sheldrick, *Acta Crystallogr., Sect. A: Found. Adv.*, 2015, **71**, 3.
51 G. M. Sheldrick, *Acta Crystallogr., Sect. C: Struct. Chem.*, 2015, **71**, 3.